Supplementary Material

Calculated Raman frequency

In contrast to the of $Ge_2Sb_2Te_5$ [40], $GeSb_4Te_7$ consists of 12 layers, including a 5-layer Sb_2Te_3 module and a 7-layer $GeSb_2Te_4$ module along the c-axis, and thus its Raman vibrational modes can be considered as a superposition of several module vibrational modes. Comparing the calculated Raman vibrational modes of Sb_2Te_3 [27], $Ge_2Sb_2Te_5$ [40], $MnBi_2Te_4$ [28], and $GeSb_4Te_7$, we found that the frequencies and vibrational modes of the $E_g(2)$ (48.4 cm^{-1}), $A_{1g}(2)$ (66.9 cm^{-1}), $E_g(4)$ (109.5 cm^{-1}), and $A_{1g}(5)$ (167.6 cm^{-1}) modes of $GeSb_4Te_7$ correspond to those of the $E_g(1)$, $A_{1g}(1)$, Eg(2), and $A_{1g}(2)$ modes of Sb_2Te_3. The frequencies of the $E_g(1)$ (35.2 cm^{-1}), $A_{1g}(1)$ (47.9 cm^{-1}), $E_g(3)$ (103.1 cm^{-1}), and $A_{1g}(3)$ (113.3 cm^{-1}) modes of $GeSb_4Te_7$ match those of the $E_g(1)$, A1g(1), $E_g(3)$, $A_{1g}(2)$, and $A_{1g}(3)$ modes of $MnBi_2Te_4$, while the $E_g(5)$ (117.2 cm^{-1}) and $A_{1g}(5)$ (170.4 cm^{-1}) modes of $GeSb_4Te_7$ are similar to the $E_g(4)$ and $A_{1g}(4)$ modes of $Ge_2Sb_2Te_5$.

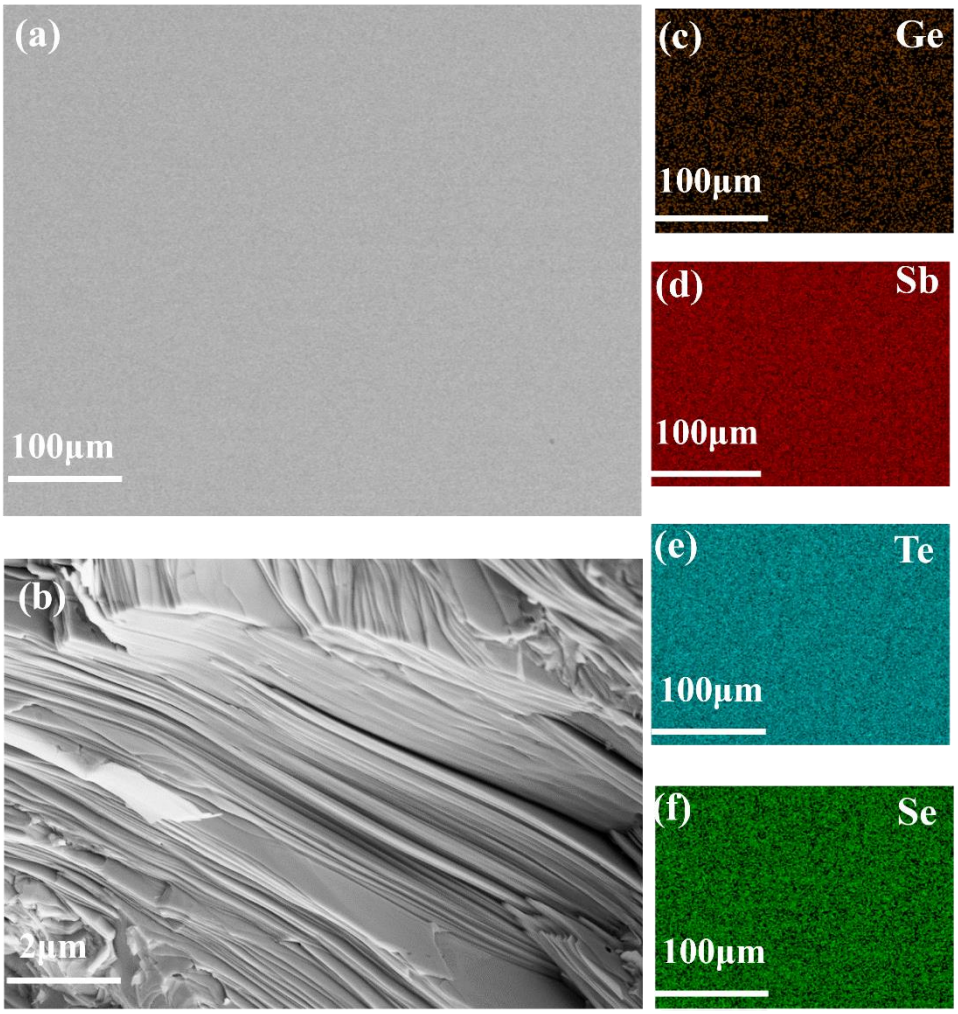

Figure S1 (a) Backscatter electron (BSE) image, (b) secondary electron (SE2) image of the fractured surface, and energy dispersive spectroscopy (EDS) mappings for (c) Ge, (d) Sb, (e) Te, (f) Se of $GeSb_4Te_5Se_2$ sample.

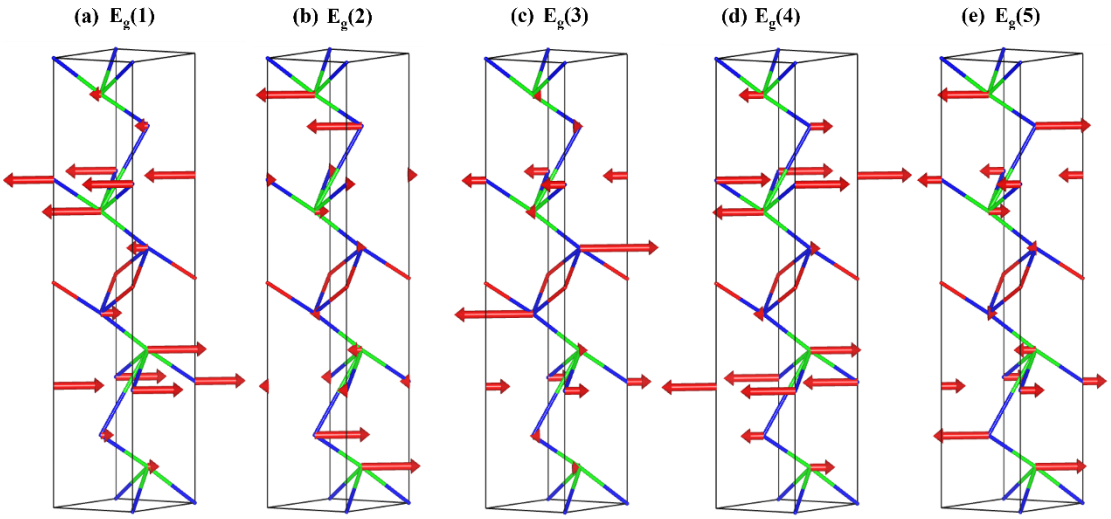

Figure S2 Sketch of the displacement patterns of Raman-active E_g phonons at the Γ-point for $GeSb_4Te_7$. Displacements along the c axis are involved.

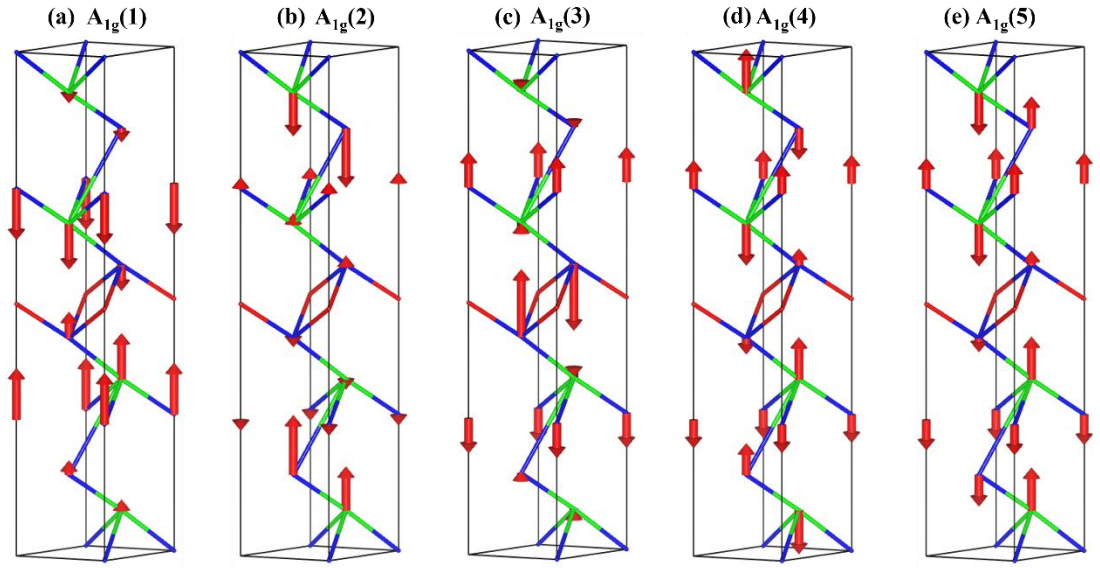

Figure S3 Sketch of the displacement patterns of Raman-active $A1_g$ phonons at the Γ-point for $GeSb_4Te_7$. Displacements along the c axis are involved.

Tabel S1 Theoretically calculated and measured frequency (cm^{-1}) of g-mode (Raman-active) phonons of the ***Γ***-point phonons for optimized geometry $GeSb_4Te_7$.

Modes	Calculated (cm^{-1})	Peak Identity	Measured (cm^{-1})
E_g(1)	35.2	-	-
A_{1g}(1)	47.9	-	-
E_g(2)	48.4	-	-
A_{1g}(2)	66.9	A	67.6
E_g(3)	103.1	B	93.6
E_g(4)	109.5	-	-
A_{1g}(3)	113.3	C	118.3
E_g(5)	117.2	--	-
-	-	D	137.9
A_{1g}(4)	167.6	E	162.9
A_{1g}(5)	170.4	-	-

Tabel S2 Peak identity of Raman spectra of $GeSb_4Te_7$.

Peak Identity	ω(cm^{-1})		Intensity		FWHM(cm^{-1})	
	value	Standard Error	value	Standard Error	value	Standard Error
Peak A	67.65	0.54	3.64	0.37	14.20	1.20
Peak B	93.58	1.02	5.64	0.79	24.71	3.99
Peak C	118.27	0.25	15.50	0.96	14.87	0.74
Peak D	137.90	0.47	8.93	0.80	17.34	1.45
Peak F	162.23	0.83	4.10	0.42	19.04	1.97

Tabel S3 C-peak Raman shifts and linewidths of $GeSb_4Te_{7-x}Se_x$ with different Se contents.

Se content x	ω(cm^{-1})		FWHM(cm^{-1})	
	value	Standard Error	value	Standard Error
0	117.09	0.13	14.85	0.74
0.1	118.26	0.24	15.39	0.48
0.2	119.30	1.17	18.42	4.25
0.3	120.42	0.63	17.45	2.76
0.5	119.18	0.29	17.00	1.08
0.8	118.07	1.30	14.81	2.45
1.5	121.29	0.29	16.72	0.92
2.0	126.04	0.38	17.75	0.99

Table S4 Direct band gap of hexagonal $GeSb_4Te_{7-x}Se_x$ compounds.

	$GeSb_4Te_{7-x}Se_x$							
Se content *x*	$x = 0$	$x = 0.1$	$x = 0.2$	$x = 0.3$	$x = 0.5$	$x = 0.8$	$x = 1.5$	$x = 2.0$
E_g (eV)	0.72*	0.69	0.72	0.73	0.63	0.64	0.63	0.63

* Data from the literature [41]

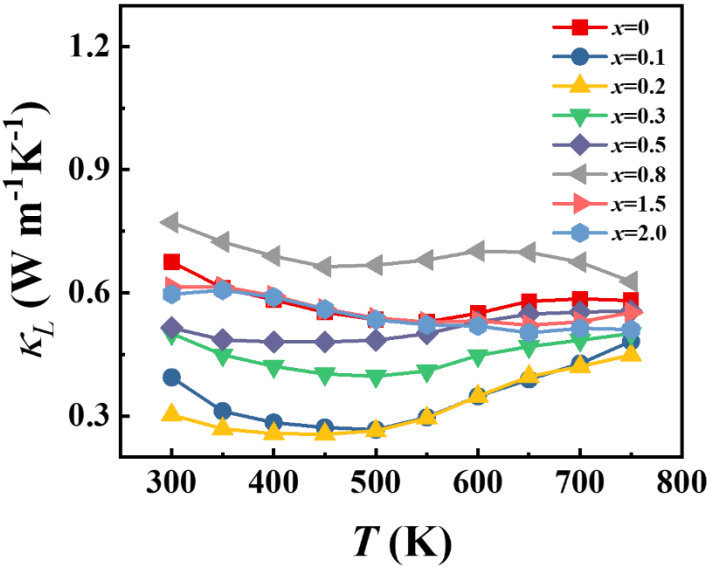

Figure S4 Temperature dependence of lattice thermal conductivity κ_L for $GeSb_4Te_{7-x}Se_x$ samples.

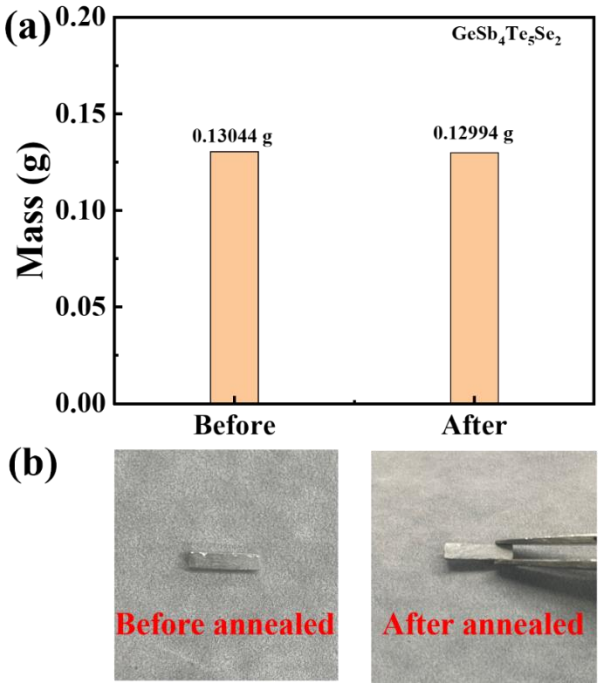

Figure S5 (a) Mass change and (b) the surface of $GeSb_4Te_5Se_2$ samples before and after annealing at 750 K.